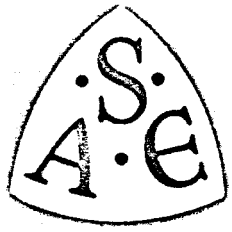

The Dynamic Stiffness of a Pneumatic Tire Model

Richard N. Dodge
Dept. of Engineering Mechanics, University of Michigan

SOCIETY OF AUTOMOTIVE ENGINEERS

Mid-Year Meeting
Chicago, Ill.
May 17-21, 1965

650491

650491

The Dynamic Stiffness of a Pneumatic Tire Model

Richard N. Dodge
Dept. of Engineering Mechanics, University of Michigan

ABSTRACT

The problem of the rotating cylindrical shell under the action of a stationary point load is treated in detail as a means of approximating the action of a tire while rolling. Comparison is made between calculated and measured load deflection curves, using a model very similar to the postulated cylindrical shell. There is reasonable correlation between such dynamic load deflection characteristics as predicted from the model and obtained experimentally, so that some support is lent to the eventual application of this model as an analog for real pneumatic tire studies.

THIS PAPER UTILIZES a rotating cylindrical shell as a model by which one may approximate the dynamic response of a real pneumatic tire. This circular cylindrical shell is presumed to have characteristics such as shown in Fig. 1, where a relatively inextensible outer band of known elastic properties is supported by an elastic foundation, which in turn is caused to rotate about a central hub. The width of this shell is considered small in comparison with its diameter or radius.

There are two reasons for studying the response of such a shell to a stationary point load. The first is that such a model may be quite easily constructed from conventional materials whose properties are well known, so that experiments may be carried out to compare the actual deflection under point load of such a model with calculations made by using the expressions developed analytically for this problem. This allows correlation between theory and experiment in a much more secure way than could be accomplished by using a real pneumatic tire. The real pneumatic tire suffers from the disadvantage of having very complex and variable elastic properties, as well as having a geometry that is not immediately susceptible to interpretation in terms of cylindrical shell dimensional parameters.

The second reason for studying such a problem is that it represents an approximation to a real pneumatic tire running under fairly light contact loads. The analytical solution of this problem, representing the light contact loads by an idealized point load, is rather straightforward and allows a fairly complete analytical solution to be obtained for this problem. Thus, one may study this problem analytically in a more thorough way than the more complicated problems

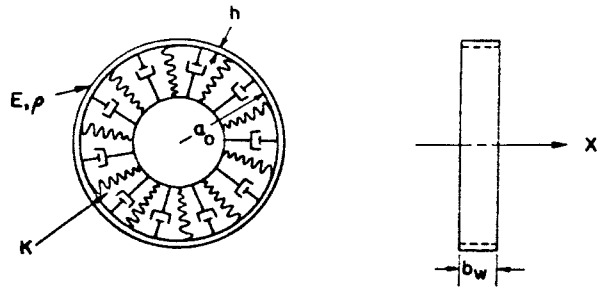

Fig. 1 - Basic cylindrical shell model for a pneumatic tire

involving finite contact area between the tire and the roadway. Details of the motion outside the contact patch may thus be examined in considerably more detail here than in other solutions. Thus, one of the primary aims of this paper is to discuss motion outside the contact patch while the tire is rolling.

The specific problem treated is that of determining expressions for the load deflection characteristics of a rotating cylindrical shell loaded by an external stationary point load. Both analytical and experimental calculations are presented for a single model.

ANALYSIS OF A ROTATING CYLINDRICAL SHELL SUPPORTED BY AN ELASTIC FOUNDATION

It has been pointed out in Refs. 1 and 2 that some hope exists that the dynamic properties of the pneumatic tire may

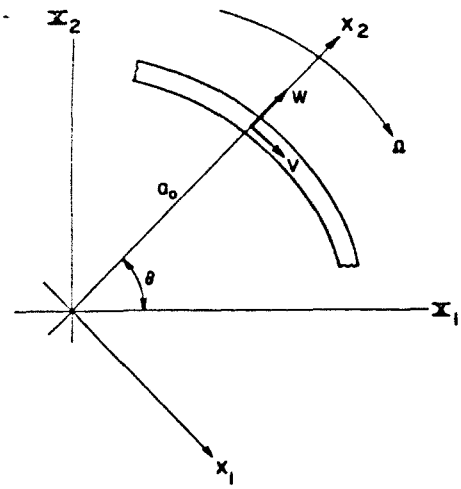

Fig. 2 - Coordinate nomenclature

be well described by the same set of equations that describes the motion of a circular cylindrical shell. One must consider the circular cylindrical shell to be internally supported by an elastic foundation such as is illustrated in Fig. 1. In this case, no loss mechanism is assumed in the generalized foundation so that its response is purely elastic.

In Fig. 2 the coordinate system shown defines the displacements associated with the circular cylindrical shell. A stationary coordinate system X_1, X_2 is fixed in space. Rotating about this origin with the rotating shell is a moving coordinate system x_1, x_2, while attached to the shell itself are the coordinates for displacement w, v in the radial and tangential directions, respectively. Eq. 1 defines certain variables used:

$$r = a + w$$

$$z = \frac{w}{a}$$

$$\psi = \frac{v}{a} \qquad (1)$$

$$\alpha^2 = \frac{h^2}{12a^2}$$

$$t = \text{time}$$

Note that the angle θ is measured relative to the moving coordinate system x_i. As has been shown in Ref. 1, the equations of motion, in terms of the moving coordinates of such a shell, are

$$\ddot{z} - \Omega(2\dot{\psi} + \Omega z + \Omega) + \frac{Eh^2}{12\rho a_0^4}(z^{IV} + 2z'' + z)$$

$$+\frac{E}{\rho a_0^2}(\psi' + z) + \frac{E}{\rho}\left(\frac{kz}{Eh}\right) = 0 \qquad (2)$$

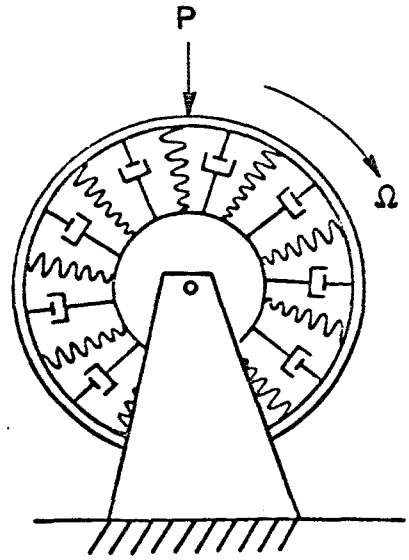

Fig. 3 - Externally applied point load to shell model

$$\ddot{\psi} - \Omega(\Omega\dot{\psi} - 2\dot{z}) - \frac{E}{\rho a_0^2}(\psi'' + z') = 0$$

The primes and dots denote differentiation with respect to θ and "t," respectively.

The development of Eqs. 2 is predicated upon the following assumptions:

1. Plane strain is assumed; that is, the strain parallel to the generators of the shell is everywhere zero.
2. Relative motion is assumed small enough so that products of displacements and their derivatives can be neglected with respect to first-order terms. This implies that Eqs. 2 are the linearized form of the equations of motion.
3. This development considers only those effects due to the deformation of the supporting elastic foundation, the deformation due to rotational effects, and local deformations due to bending. Damping has not been included.
4. Lateral contraction of the shell parallel to the generators has been neglected for convenience.

In Eqs. 2, "k" represents the local spring constant per unit area of the supporting elastic foundation, ρ is the mass density of the shell band, E is the extension modulus of the shell band, and Ω is the constant angular velocity of the combined shell and its supporting foundation.

POINT-LOAD PROBLEM

The point-load geometry is illustrated in Fig. 3, where it is seen that a concentrated load P is applied to the model at a fixed point in space. In order to cause this point in space to remain fixed, it is convenient to introduce the new coordinates

$$t_1 = t \qquad \theta_1 = \theta + \Omega t \qquad (3)$$

By use of such coordinates, it may be seen that the load P may be applied at the point $\theta_1 = 0$, which now corresponds to a fixed point in space. Eqs. 2 may be expressed in terms of these new coordinates. Omitting the details of such a transformation, one obtains from Eqs. 2:

$$\ddot{z} + 2\Omega\dot{z}' + \Omega^2 z'' - \Omega[2(\dot{\psi} + \Omega\psi') + \Omega z + \Omega] + \frac{Eh^2}{12\rho a_0^4}(z^{IV} + 2z'' + z) + \frac{E}{\rho a_0^2}(\psi' + z) + \frac{E}{\rho}\frac{kz}{Eh} = 0 \tag{4}$$

$$\ddot{\psi} + 2\Omega\dot{\psi}' + \Omega^2\psi'' - \Omega[\Omega\psi - 2(\dot{z} + \Omega z')] - \frac{E}{\rho a_0^2}(\psi'' + z') = 0$$

where dots and primes now indicate differentiation with respect to t_1 and θ_1, respectively.

We are interested here in steady-state running conditions, in which case the transient terms of Eqs. 4 vanish, since they represent transients with respect to our $\theta_1 - t_1$ coordinate system, a system that is now fixed in space. The omission of time dependent terms of Eqs. 4 results in a steady-state equation that describes the geometry of the standing waves in the rotating shell with respect to the θ_1, or fixed, coordinate system. Such equations become

$$z^{IV} + \left(2 + \frac{\bar{w}^2}{\alpha^2}\right)z'' + \left(1 + \frac{\bar{k}}{a^2} + \frac{1}{\alpha^2} - \frac{\bar{w}^2}{\alpha^2}\right)z + \left(\frac{1}{\alpha^2} - \frac{2\bar{w}^2}{\alpha^2}\right)\psi' = \frac{\bar{w}}{\alpha^2} \tag{5}$$

$$\left(\frac{\bar{w}^2}{\alpha^2} - \frac{1}{\alpha^2}\right)\psi''' - \frac{\bar{w}^2}{\alpha^2}\dot{\psi} - \left(\frac{1}{\alpha^2} - \frac{2\bar{w}^2}{\alpha^2}\right)z' = 0$$

where

$$\bar{w}^2 = \frac{\Omega^2 a_0^2 \rho}{E} \qquad \bar{k} = \frac{ka_0^2}{Eh}$$

In view of the fact that the coefficients of "z" and its derivatives are constant for constant Ω, ρ, h, a_0, and E, Eqs. 5 take the form:

$$z^{IV} + A_1 z'' + A_2 z + A_3\psi' = A_4$$
$$A_5\psi'' - A_4\psi - A_3 z' = 0 \tag{5a}$$

The quantity ψ may be eliminated from Eqs. 5a, yielding a single sixth-order differential equation in the radial dimensionless displacement "z."

$$z^{VI} + H_1 z^{IV} + H_2 z'' - H_3 z = -H_4 \tag{6}$$

where:

$$H_1 = \frac{\bar{w}^2}{\alpha^2}\left[1 - \frac{\alpha^2}{(\bar{w}^2 - 1)}\right] + 2$$

$$H_2 = 1 + \frac{\bar{k}}{\alpha^2} + \frac{1}{\alpha^2} - \frac{\bar{w}^2}{\alpha^2}\left[1 + \frac{(2\alpha^2 + \bar{w}^2)}{(\bar{w}^2 - 1)}\right] + \frac{(1 - 2\bar{w}^2)^2}{\alpha^2(\bar{w}^2 - 1)}$$

$$H_3 = \frac{\bar{w}^2}{(\bar{w}^2 - 1)}\left[1 + \frac{\bar{k}}{\alpha^2} + \frac{1}{\alpha^2} - \frac{\bar{w}^2}{\alpha^2}\right] \tag{7}$$

$$H_4 = \frac{(\bar{w}^2)^2}{\alpha^2(\bar{w}^2 - 1)}$$

A particular solution of Eq. 6 is

$$z_p = \frac{-H_4}{-H_3} = \frac{\bar{w}^2/\alpha^2}{1 + (\bar{k}/\alpha^2) + (1/\alpha^2) - (\bar{w}^2/\alpha^2)} \tag{8}$$

If the solution to the homogeneous equation formed from Eq. 6 is assumed to be of the type $z_c = Ae^{q\theta_1}$, then the characteristic equation for "q" is

$$q^6 + H_1 q^4 + H_2 q^2 - H_3 = 0 \tag{9}$$

This may be rewritten as

$$Q^3 + H_1 Q^2 + H_2 Q - H_3 = 0 \tag{10}$$

where $Q = q^2$.

Upon consideration of the form of H_1, H_2, and H_3, it may be shown that the solutions of Eq. 10 consist of one negative root (Q_1) and a pair of complex conjugate roots (Q_2 and

Q_3). The root Q_1 leads to pure imaginary "q," while Q_2 and Q_3 lead to a pair of complex conjugate "q"s. These roots are represented as

$$q_{1-2} = \pm ib_1 \text{ from } Q_1$$

$$q_{3-4} = \pm (a_2 + ib_2) \text{ from } Q_2$$

$$q_{5-6} = \pm (a_2 - ib_2) \text{ from } Q_3$$

Thus the homogeneous solution of Eq. 6 is

$$z_c = C_1 \cos b_1\theta_1 + C_2 \sin b_1\theta_1 + e^{a_2\theta_1}[C_3 \cos b_2\theta_1 + C_4 \sin b_2\theta_1] + e^{-a_2\theta_1}[C_5 \cos b_2\theta_1 + C_6 \sin b_2\theta_1] \tag{11}$$

It is instructive to view Eq. 11 first from the point of view of angles θ_1 lying between 0 and π. In this region of positive angle, one physically expects the effects of the point load to be relatively small at the upper surface of the shell denoted by $\theta_1 = \pi$. This leads immediately to the realization that the constants C_3 and C_4 of Eq. 11 must be very small. Further, if we restrict attention primarily to the region θ_1 small, then the effect of the small constants C_3 and C_4 upon the overall solution must be nearly negligible.

By such a line of reasoning, one may separate out Eq. 11 into two portions, one valid for positive angles, or forward of the point of load application, and the second portion valid aft of the point of load application, say, in the region θ_1 up to $-\pi$. This is expressed analytically in Eqs. 12a and 12b.

For $0 < \theta_1 < \pi$,

$$z_1 = C_1 \cos b_1\theta_1 + C_2 \sin b_1\theta_1 + e^{-a_2\theta_1}[C_5 \cos b_2\theta_1 + C_6 \sin b_2\theta_1] \tag{12a}$$

For $-\pi < \theta_1 < 0$,

$$z_2 = C_1 \cos b_1\theta_1 + C_2 \sin b_1\theta_1 + e^{a_2\theta_1}[C_3 \cos b_2\theta_1 + C_4 \sin b_2\theta_1] \tag{12b}$$

The constants appearing in Eqs. 12a and 12b may be evaluated by using equations expressing the continuity of the dimensionless deflection and its derivatives across the load point, as well as the continuity of such quantities at the upper edge of the shell. These are given in Eqs. 13a, b, c, d, e, and f:

$$z_1(\theta_1 = \dot{0}) - z_2(\theta_1 = \bar{0}) = 0 \tag{13a}$$

$$z_1'(\dot{0}) - z_2'(\bar{0}) = 0 \tag{13b}$$

$$z_1''(\dot{0}) - z_2''(\bar{0}) = 0 \tag{13c}$$

$$z_1'''(\dot{0}) - z_2'''(\bar{0}) = 2P^* \tag{13d}$$

$$z_1(+\pi^-) - z_2(-\pi^+) = 0 \tag{13e}$$

$$z_1'(+\pi^-) - z_2'(-\pi^+) = 0 \tag{13f}$$

where:

$$P^* = \frac{6a_0^2 p}{b_w \cdot Eh^3}$$

Note that Eq. 13a represents continuity of displacement at $\theta_1 = 0$, Eq. 13b represents continuity of slope, Eq. 13c continuity of bending moment, and Eq. 13d indicates that the sum of the shear forces is equal to the total applied force P. Eqs. 13e and 13f represent continuity of displacement and slope at the point $\theta_1 = \pi$ or $-\pi$. Using these conditions, along with the solutions of Eqs. 12, the constants C_3, C_4, C_5, and C_6 are found to be

$$C_3 = C_5 = \frac{P^*}{2a_2(b_2^2 + a_2^2)}$$

$$C_6 = -C_4 = \frac{P^*}{2b_2(b_2^2 + a_2^2)} \tag{14a}$$

and from Eqs. 13e and 13f

$$C_2 = 0$$

$$C_1 = \frac{e^{-a_2\pi}[\sin(b_2\pi)]P^*}{-2b_1a_2b_2\sin(b_1\pi)} \tag{14b}$$

Combining Eqs. 8, 12, and 14 gives finally solutions for the dimensionless deformation "z" due to a point load ap-

plied at $\theta_1 = 0$ in the form

$$z_1 = \frac{P^*}{2}\left\{\frac{e^{-a_2\pi}\,[\sin(b_2\pi)]\cos b_1\theta_1}{-b_1 a_2 b_2 \sin(b_1\pi)} + \left[\frac{e^{-a_2\theta_1}}{(b_2^2 + a_2^2)}\right] \times \left[\frac{1}{a_2}\cos b_2\theta_1 + \frac{1}{b_2}\sin b_2\theta_1\right]\right\} + \frac{\bar{w}^2/\alpha^2}{1 + (\bar{k}/\alpha^2) + (1/\alpha^2) - (\bar{w}^2/\alpha^2)} \qquad 0 < \theta_1 < \pi \tag{15a}$$

$$z_2 = \frac{P^*}{2}\left\{\frac{e^{-a_2\pi}\,[\sin(b_2\pi)]\cos b_1\theta_1}{-b_1 a_2 b_2 \sin(b_1\pi)} + \frac{e^{a_2\theta_1}}{b_2^2 + a_2^2}\left[\frac{1}{a_2}\cos b_2\theta_1 - \frac{1}{b_2}\sin b_2\theta_1\right]\right\} + \frac{\bar{w}^2/\alpha^2}{1 + (\bar{k}/\alpha^2) + (1/\alpha^2) - (\bar{w}^2/\alpha^2)} \qquad -\pi < \theta_1 < 0 \tag{15b}$$

Note that it is rather difficult to interpret the influence of any single parameter upon the load deflection relationships as given by Eqs. 15, since almost all the quantities entering into these relationships are derived from the cubic Eq. 10, whose solutions are difficult to estimate in terms of the input parameters. However, the calculations that have been done seem to indicate the following results, given with the restriction that they may not represent general conclusions but are rather specific conclusions for the model used later on in the experimental studies:

1. At a given value of load P^*, the deflection "z" at the point $\theta_1 = 0$ increases slightly as speed increases, since the quantity a_2 in the denominator decreases more rapidly than the quantity $(a_2^2 + b_2^2)$ increases.

2. The first term of Eq. 15a represents an undamped harmonic wave that travels completely around the circumference of the shell. The magnitude of this wave starts with a negative value, but increases with speed so that it moves closer toward zero. It would be expected that at high speeds this magnitude would pass through zero and become a larger positive number.

3. The second term of Eq. 15a represents a damped harmonic wave with maximum amplitude at the point of load application. The damping constant a_2 decreases as the angular velocity increases, so that the wave becomes more pronounced around a greater portion of the circumference of the shell.

4. It will be recognized that identical conclusions hold for Eq. 15b as well as Eq. 15a.

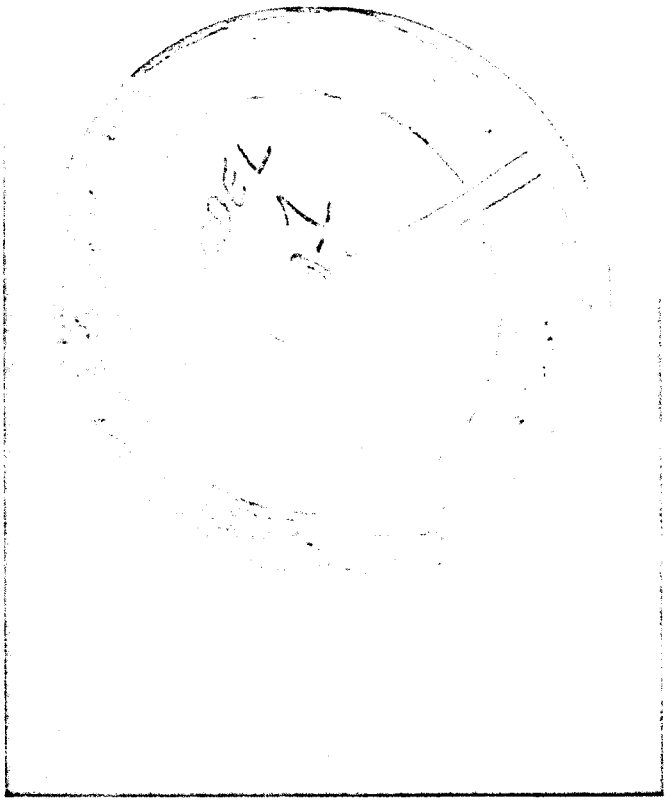

Fig. 4 - Experimental test model

EXPERIMENTAL MEASUREMENTS

A model designed to provide a means of conducting simple experiments verifying the applicability of Eqs. 15a and 15b was built, and is illustrated in Fig. 4, where the model elastic constants are $k = 27$ lb/in.^{3}, $Eh^3 = 55$ lb-in., $\alpha^2 = 3.121 \times 10^{-5}$, $a_0 = 3.875$ in., and $\rho h = 1.51 \times 10^{-5}$ slug-ft/in.^{3}. The cylindrical shell used here is made of a thin rubber belt reinforced with twisted steel cords wrapped in the circumferential direction, and is merely the core of an ordinary timing belt. The elastic foundation consists of a sponge rubber insert bonded to the belt with silicone rubber. This elastic foundation is attached to a central hub of plexiglass and aluminum.

Table 1 gives load deflection data taken on the model in a stationary position and under a point load at $\theta_1 = 0$. The test stand used for these experiments is illustrated in Fig. 5. It consists of a variable speed motor for controlling the angular velocity, a pivoted arm for applying the load, a ball bearing roller to serve as the loading point, and a load

Table 1 - Point Load versus Deflection at Ω = 400 rpm

Load, lb	Deflection, in.
0	0
-1.	-0.021
-2.	-0.041
-3.	-0.061
-4.	-0.079
-5.	-0.095
-6.	-0.119
-7.	-0.145
-8.	-0.171
-9	-0.198

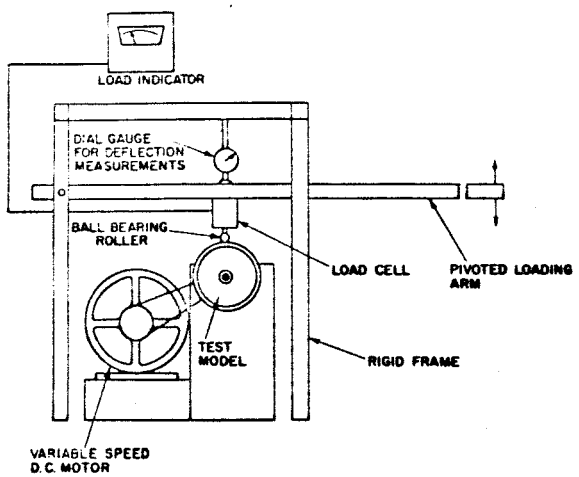

Fig. 5 - Schematic of test stand

cell for measuring magnitude of the applied load. A mechanical dial gage records the deflection of this load.

In collecting these data, the deflection measurements were made after the model was running at its prescribed angular velocity. This introduced a slight error when such measurements were compared with calculations done on the basis of Eqs. 15a and 15b, since these do not include the deformation due to pure rotational effects. However, as can be seen from the calculations, the deformation due to these effects was very small compared with the bending deformation.

An additional error was introduced because the roller representing the point load was a finite radius of curvature. This caused the contact to be over some length, a situation not contemplated in the analytical solution given by Eqs. 15. However, comparison between static load deflection data taken with the model loaded against a sharp edge and loaded against the roller used here seems to indicate that the differences between the two load deflections should be negligible.

Typical load deflection data taken from the rotating shell

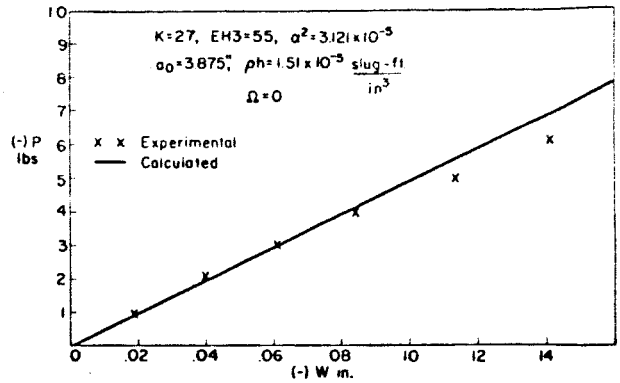

Fig. 6 - Load versus deflection, test model 1, Ω = 0

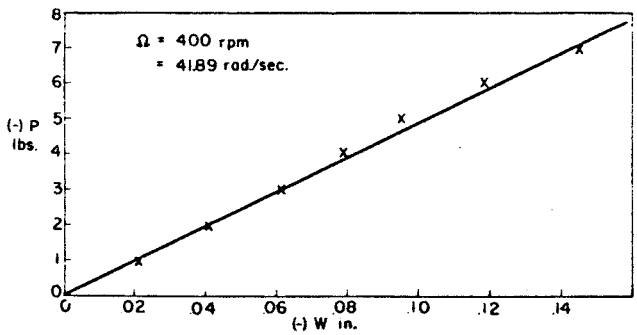

Fig. 7 - Load versus deflection, test model 1, Ω = 400 rpm

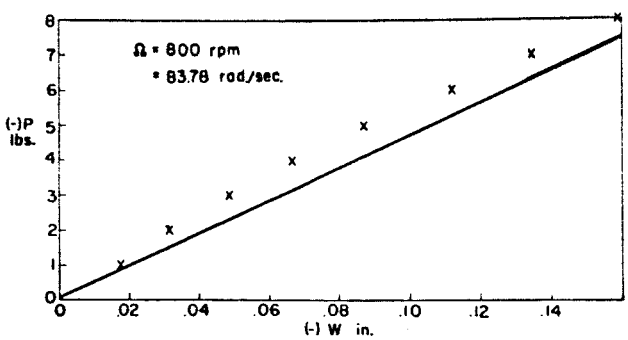

Fig. 8 - Load versus deflection, test model 1, Ω = 800 rpm

model are shown in Figs. 6-10. Load deflection curves predicted from Eqs. 15 are also given for these same tests as solid lines on the figures. Note that, in general, agreement seems to be reasonably good, since the elastic data for the model were obtained by separate measurements of its components before assembly. Calculations made on the basis of Eqs. 15 seem to be somewhat less successful at higher rotating speeds, and further work on these dynamic effects is probably necessary.

In general, one would expect the deflection of such a system to increase with speed under a constant load, but as has been pointed out by Kenney in Ref. 4, by increasing surface speed, one is moving up the left-hand branch of a simple resonance diagram corresponding to the equality of surface

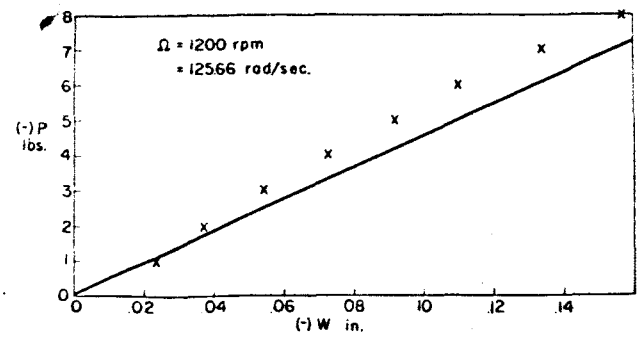

Fig. 9 - Load versus deflection, test model 1, Ω = 1200 rpm

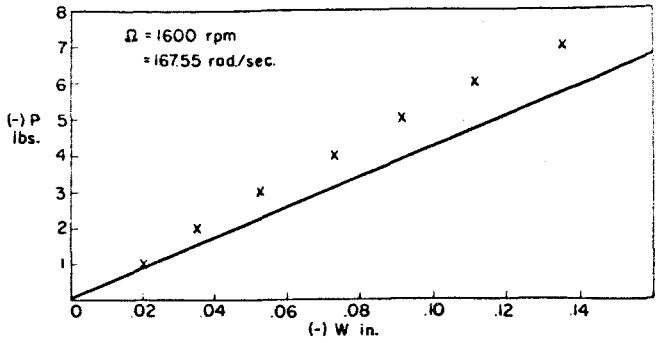

Fig. 10 - Load versus deflection, test model 1, Ω = 1600 rpm

speed with the wave propagation velocity for bending disturbances. That particular resonant condition should result, in the undamped case, in indefinitely large deflections per unit load so that in general the deflections should be increasing.

REFERENCES

1. S. K. Clark, "An Analog for the Static Loading of a Pneumatic Tire," The University of Michigan, Office of Research Administration, Technical Report 02957-19-T, Ann Arbor, Michigan, March 1964.

2. J. T. Tielking, "Plane Vibration Characteristics of a Pneumatic Tire Model." Paper 650492 presented at SAE Mid-Year Meeting, Chicago, May 1965.

3. R. A. DiTaranto and M. Lessen, "Coriolis Acceleration Effect on the Vibration of a Rotating Thin-Walled Circular Cylinder," J. Appl. Mechanics (December 1964), 700.

4. J. T. Kenney, "Steady-State Vibrations of Beam on Elastic Foundation for Moving Load," J. Appl. Mechanics (December 1954), 359.

5. V. Z. Vlasov, "General Theory of Shells and Its Applications in Engineering," NASA Publication, p. 290.